SLAC-PUB-5881
August 1992
(A)

A FINITE ELEMENT FIELD SOLVER FOR DIPOLE MODES*

E. M. Nelson

Stanford Linear Accelerator Center
Stanford University, Stanford, California 94309 USA

Abstract

A finite element field solver for dipole modes in axisymmetric structures has been written. The second-order elements used in this formulation yield accurate mode frequencies with no spurious modes. Quasi-periodic boundaries are included to allow travelling waves in periodic structures. The solver is useful in applications requiring precise frequency calculations such as detuned accelerator structures for linear colliders. Comparisons are made with measurements and with the popular but less accurate field solver URMEL[1].

Introduction

The finite element field solver YAP[2] has been extended to calculate dipole modes to aid the design of detuned accelerator structures. The detuned accelerator structure is a disk loaded waveguide with cell parameters (diameter $2b$, disk aperture $2a$ and disk thickness t) varying along the structure such that the lowest synchronous dipole modes of the cells have a gaussian density distribution while keeping the phase velocity of the accelerating mode constant. The formulation described here yields the synchronous dipole mode frequency with accuracy better than 30 ppm. An accuracy less than 10^{-4} is desired. Combined with YAP's high accuracy monopole field solutions for the accelerating mode, the parameters of the detuned structure can be determined with errors less than machining tolerances. This design process requires only minimal cold-testing and furthermore, with precision machining, it could eliminate the need to tune each cell of the structure.

This paper describes the finite element formulation used to calculate the dipole modes and then presents some test results verifying its accuracy.

Finite Element Formulation

This paper describes an algorithm for finding the magnetic field $\mathbf{B}$. Changing the boundary conditions on the metal walls will yield the electric field $\mathbf{E}$ instead. The magnetic field $\mathbf{B}$ has three components B_z, B_ρ and B_ϕ which have an assumed time dependence $e^{-i\omega t}$ and azimuthal dependence $e^{im\phi}$ with $m = 1$. Modification of the boundary conditions and elements on the axis will allow solutions for $m \neq 1$. The interior of the structure in the (z, ρ) plane is Ω. Consider four types of boundaries: Γ_{metal}, Γ_{axis}, Γ_{left} and Γ_{right}. The last two boundaries are the left and right boundaries of one cell of a periodic structure. They are connected by a z translation operator, $R : \Gamma_{\text{left}} \rightarrow \Gamma_{\text{right}}$. The fields in a periodic structure are decomposed into modes with phase advance ψ in accordance with Floquet's theorem. Symmetry boundaries are also available.

Strong Formulation

Combining Maxwell's curl equations yields the following strong formulation for dipole modes: given the phase advance ψ, find the eigenvalues ω^2/c^2 and eigenmodes $\mathbf{B}$ such that

$$\nabla \times (\nabla \times \mathbf{B}) - \frac{\omega^2}{c^2}\mathbf{B} = 0 \quad \text{in } \Omega, \tag{1a}$$

$$\hat{n} \times (\nabla \times \mathbf{B}) = 0 \quad \text{on } \Gamma_{\text{metal}}, \tag{1b}$$

$$B_z = 0 \quad \text{and} \quad B_\phi = iB_\rho \quad \text{on } \Gamma_{\text{axis}}, \tag{1c}$$

$$\hat{n} \times (\nabla \times \mathbf{B})|_{R\mathbf{x}} = -\hat{n} \times (\nabla \times \mathbf{B})|_{\mathbf{x}} e^{i\psi}$$
$$\text{and} \quad \mathbf{B}(R\mathbf{x}) = \mathbf{B}(\mathbf{x})e^{i\psi} \quad \forall \mathbf{x} \in \Gamma_{\text{left}}. \tag{1d}$$

This formulation does not include all of Maxwell's equations. In particular, there are irrotational solutions with $\omega = 0$. These unphysical solutions are separate from the desired solenoidal solutions which have $\omega > 0$. For solenoidal solutions, the boundary condition (1b) corresponds to $\hat{n} \times \mathbf{E} = 0$ and also implies $\hat{n} \cdot \mathbf{B} = 0$ on Γ_{metal}. Boundary condition (1c) states that $\mathbf{B}$ is continuous at the axis, and boundary condition (1d) is the quasi-periodic boundary condition for periodic structures.

Weak Formulation

The equivalent weak, or variational, formulation of the problem is: given the phase advance ψ, find ω^2/c^2 and $\mathbf{B} \in \mathcal{V}$ such that for all test fields $\mathbf{C} \in \mathcal{V}$,

$$\int_\Omega (\nabla \times \mathbf{C})^* \cdot (\nabla \times \mathbf{B}) - \frac{\omega^2}{c^2}\mathbf{C}^* \cdot \mathbf{B}\, \rho d\Omega = 0 \tag{2a}$$

where

$$\mathcal{V} = \{\mathbf{A} \in H(\text{curl}) :$$
$$\mathbf{A}(R\mathbf{x}) = \mathbf{A}(\mathbf{x})e^{i\phi} \quad \forall \mathbf{x} \in \Gamma_{\text{left}}, \tag{2b}$$
$$A_z = 0 \quad \text{and} \quad A_\phi = iA_\rho \quad \text{on } \Gamma_{\text{axis}}\}.$$

The set $H(\text{curl})$ contains all vector fields $\mathbf{A}$ for which the integral (2a) with $\mathbf{C} = \mathbf{B} = \mathbf{A}$ exists. This condition constrains the tangential component of $\mathbf{A}$ (i.e., $\mathbf{B}$ and $\mathbf{C}$) to be continuous across an interface, for example between two elements. There is no such constraint on the component of the field normal to an interface, but the finite element solutions below yield normal components of the field which are near continuous.

* Work supported by Department of Energy, contract DE-AC03-76SF00515.

Presented at Linac '92 Conference, Ottawa, Canada, August 24-28, 1992

Finite Element Formulation

In order to solve for the fields on a computer, a finite dimensional subspace $\mathcal{V}_h \subset \mathcal{V}$ is used in the weak formulation above. A field $\mathbf{A} \in \mathcal{V}_h$ is a linear combination of basis functions. Texts such as Strang and Fix[3] and Hughes[4] describe the finite element method, where the basis functions are assembled from simple functions on each element.

In YAP, the domain Ω is partitioned into triangular elements, as in the example shown in figure 1(a). For each element there is a map $\mathbf{x}_e : \widehat{\Omega} \to \Omega_e$ which is used to transforms integrals over Ω_e to integrals over the master element $\widehat{\Omega}$ shown in figure 1(b). Quadratic maps are used to approximate curved boundaries well. Let the coordinates of a point in $\widehat{\Omega}$ be r and s. The map for element e gives $(z, \rho) = \mathbf{x}_e(r, s)$.

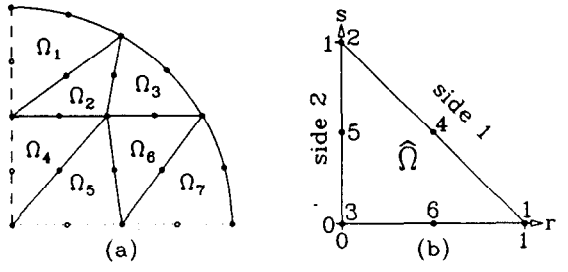

Fig. 1 (a) A sphere partitioned into elements. The dotted line is the axis and the dashed line is a symmetry plane. (b) The master element $\widehat{\Omega}$ and its 6 nodes.

The finite element basis is inspired by the works of Crowley[5] and Nedelec[6]. There are 14 basis functions for elements which are not adjacent to the axis, such as Ω_1, Ω_2 and Ω_3 in figure 1(a). On such elements the field $-i\rho B_\phi$ is represented by the usual quadratic lagrangian basis functions

$$\begin{array}{lll} N_1 = r(2r-1) & N_2 = s(2s-1) & N_3 = t(2t-1) \\ N_4 = 4rs & N_5 = 4st & N_6 = 4rt \end{array} \tag{3}$$

where $t = 1 - r - s$. In a typical application of the finite element method, the lagrangian basis functions would also be used for B_z and B_ρ, but this leads to difficulties with spurious modes. Instead, YAP constructs vector basis functions for (B_z, B_ρ) as follows. Given the element map $\mathbf{x}_e : \widehat{\Omega} \to \Omega_e$, the vectors $\mathbf{V}_i$ tangential to side i are

$$\mathbf{V}_1 = -(\mathbf{V}_2 + \mathbf{V}_3) \quad \mathbf{V}_2 = -\frac{\partial \mathbf{x}_e}{\partial s} \quad \mathbf{V}_3 = \frac{\partial \mathbf{x}_e}{\partial r}. \tag{4}$$

The reciprocal vectors $\mathbf{R}_i$ normal to side i are

$$\begin{aligned} \mathbf{R}_1 &= -(\mathbf{R}_2 + \mathbf{R}_3) \\ \mathbf{R}_2 &= \frac{\hat{\phi} \times \mathbf{V}_2}{\hat{\phi} \cdot (\mathbf{V}_2 \times \mathbf{V}_3)} \\ \mathbf{R}_3 &= \frac{\hat{\phi} \times \mathbf{V}_3}{\hat{\phi} \cdot (\mathbf{V}_2 \times \mathbf{V}_3)}. \end{aligned} \tag{5}$$

Then a set of vector fields easily assembled into $H(\text{curl})$ are constructed. The fields $\mathbf{L}_i$ satisfying $\mathbf{L}_i \cdot \mathbf{V}_j = \delta_{ij}$ on the sides of the element are

$$\mathbf{L}_1 = r\mathbf{R}_3 - s\mathbf{R}_2 \quad \mathbf{L}_2 = s\mathbf{R}_1 - t\mathbf{R}_3 \quad \mathbf{L}_3 = t\mathbf{R}_2 - r\mathbf{R}_1. \tag{6}$$

Finally, the 8 vector basis functions are

$$\begin{array}{lll} \mathbf{N}_7 = r\mathbf{L}_1 & \mathbf{N}_{10} = t\mathbf{L}_2 & \mathbf{N}_{13} = -2s\mathbf{L}_3 \\ \mathbf{N}_8 = s\mathbf{L}_1 & \mathbf{N}_{11} = t\mathbf{L}_3 & \mathbf{N}_{14} = -2t\mathbf{L}_1. \\ \mathbf{N}_9 = s\mathbf{L}_2 & \mathbf{N}_{12} = r\mathbf{L}_3 & \end{array} \tag{7}$$

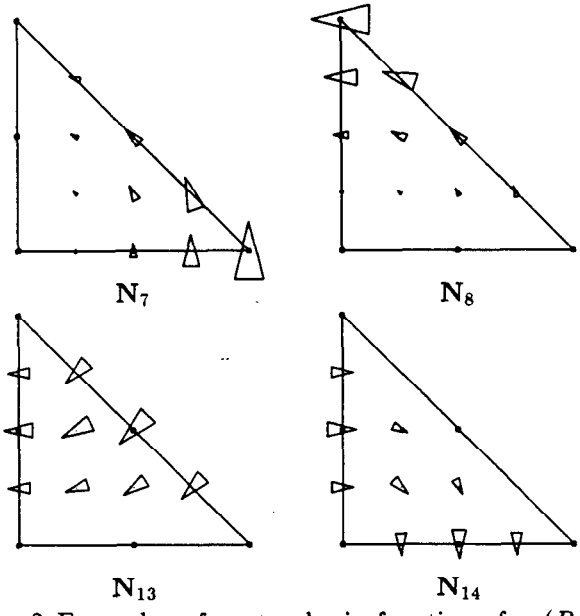

Fig. 2 Examples of vector basis functions for (B_z, B_ρ). The size and direction of the arrows indicate the magnitude and direction of the basis functions.

Elements which touch the axis must enforce the boundary conditions there. Elements with one corner on the axis, such as Ω_4 and Ω_6 in figure 1(a), have 11 basis functions. Assuming node 2 on axis, the basis functions in the form $((B_z, B_\rho), -i\rho B_\phi)$ are

$$\begin{array}{ll} \mathbf{N}_1 = (\mathbf{0}, r(2r-1) + rs) & \mathbf{N}_6 = (r\mathbf{L}_1, 0) \\ \mathbf{N}_2 = (\mathbf{0}, t(2t-1) + st) & \mathbf{N}_7 = (t\mathbf{L}_2, 0) \\ \mathbf{N}_3 = (\mathbf{0}, 4rt) & \mathbf{N}_8 = (t\mathbf{L}_3, 0) \\ \mathbf{N}_4 = (-s\mathbf{L}_1, rs) & \mathbf{N}_9 = (r\mathbf{L}_3, 0) \\ \mathbf{N}_5 = (s\mathbf{L}_2, st) & \mathbf{N}_{10} = (-2s\mathbf{L}_3, 0) \\ & \mathbf{N}_{11} = (-2t\mathbf{L}_1, 0). \end{array} \tag{8}$$

Elements with one side on the axis, such as Ω_5 and Ω_7 in figure 1(a), have 6 basis functions. Assuming side 3 on axis, they are

$$\begin{array}{ll} \mathbf{N}_1 = (\mathbf{0}, s^2) & \mathbf{N}_4 = (s\mathbf{L}_1, 0) \\ \mathbf{N}_2 = (r\mathbf{R}_3, rs) & \mathbf{N}_5 = (s\mathbf{L}_2, 0) \\ \mathbf{N}_3 = (t\mathbf{R}_3, st) & \mathbf{N}_6 = (-2s\mathbf{L}_3, 0). \end{array} \tag{9}$$

The field **B** is a linear combination of these basis functions. Substituting these fields into (2a) yields a generalized eigenvalue problem which can be solved for the approximate eigenvalues ω^2/c^2 and eigenvectors **B**. Careful orientation of the vector basis functions is necessary to ensure that the tangential component of the field is continuous across the element boundaries. This and the quasi-periodic boundary condition are handled when assembling the element matrices (the integral (2a) restricted to Ω_e) into the global matrices (the integral (2a) over all of Ω).

Tests

Tests on the lowest mode of a pillbox and the second lowest mode of a sphere are shown in figure 3. A pillbox 1cm high with a 1cm radius has eigenvalue $\omega^2/c^2 = 13.25956212\,\mathrm{cm}^{-2}$ for the lowest mode. A sphere with radius of 1cm has $\omega^2/c^2 = 14.97874667\,\mathrm{cm}^{-2}$ for the second lowest mode. The results show that YAP can provide higher accuracy by over an order of magnitude. The relative error in the eigenvalue scales as $\mathcal{O}(h^{3.8})$ for YAP, $\mathcal{O}(h^2)$ for URMEL on a pillbox, and $\mathcal{O}(h)$ for URMEL on a sphere. Inadequate modelling of curved boundaries is responsible for the poor scaling observed in URMEL on a sphere.

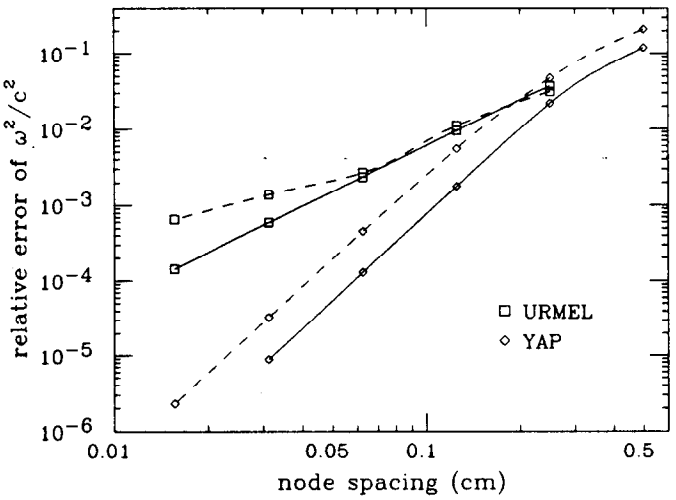

Fig. 3 Test on a pillbox (solid line) and a sphere (dashed line).

Careful choice of the basis functions makes this finite element formulation preserve the continuum result that all unphysical solutions have $\omega = 0$, so the spurious solutions which plague many field solvers are easily avoided[7]. A naive choice for the basis functions often leads to a finite element field solver which is unreliable due to the presence of spurious modes with $\omega > 0$.

X Band Accelerator Structure

An example of an x-band accelerator structure is shown in figure 4. The estimated relative error for the calculated frequency for the lowest dipole π mode using this mesh is 0.0033, and refining the mesh reduces the frequency error to 10 ppm. This is an estimated error of 150 KHz relative to the lowest dipole π mode frequency of 15 GHz. Measurements on a stack of six identical cells (five cells with a shorted half-cell on each end) agree with the calculations. For example, the second lowest dipole 0 mode frequency was calculated to be 16.764 GHz. Compared with the measured frequency of 16.761 GHz, the error is 3 MHz, or 200 ppm. This is consistent with the 100 ppm error estimate for the dimensions of the structure and the 1 MHz error estimate for the frequency measurement.

These results demonstrate that YAP can find mode frequencies to a high degree of accuracy. In particular, it has sufficient accuracy to aid the design of detuned accelerator structures.

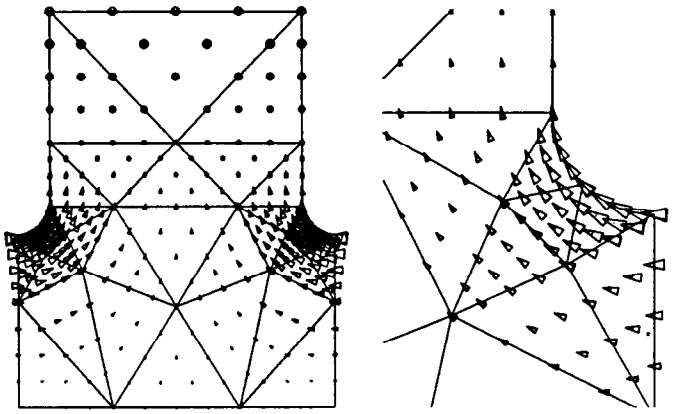

Fig. 4 (a) Lowest dipole π mode for an x-band accelerator structure and (b) magnified view of the right nose. The arrows represent the field (B_z, B_ρ) and the circles represent the field $-i\rho B_\phi$. The sizes of the circles and arrows indicate the magnitude of the fields.

References

[1] T. Weiland, "On the Computation of Resonant Modes in Cylindrically Symmetric Cavities," Nuclear instruments and Methods **216**, pp 329-348 (1983)

[2] E. Nelson, "A 2d Field Solver for Periodic Structures with Special Corner Elements," SLAC-PUB-5532 or Proc. 1991 IEEE Particle Accelerator Conference, pp 722-724.

[3] Strang and Fix, An Analysis of the Finite Element Method, Prentice Hall, 1973

[4] Hughes, The Finite Element Method, Prentice Hall, 1987

[5] C.W. Crowley, P.P. Silvester, H. Hurwitz Jr., "Covariant Projections Elements for 3D Vector Field Problem," IEEE Trans. on Magnetics, MAG-24, No. 1, pp. 397-400, 1988

[6] J.C. Nedelec, "Mixed Finite Elements in $\mathbf{R}^3$," Num. Math., vol 35, pp. 315-341, 1980

[7] A.R. Pinchuk, C.W. Crowley, P.P. Silvester, "Spurious Solutions to Vector Diffusion and Wave Field Problems," IEEE Trans. on Magnetics, MAG-24, No. 1, pp. 158-161, 1988